Article

Spatiotemporal Variability Analysis of Glaciers in the Hindukush Region of Pakistan using Remote Sensing Data

Muhammad Irfan[1], Jabir Hussain Syed[2], Ahsan Riaz Khan* Mehrab Khan[1], Muhammad Shafi[3], Hamid Iqbal[4,5], Muhammad Usman Hanif[3,6] and Yasmeen Nargis[7]

[1]Department of Earth and Environmental Sciences, Bahria University Karachi, Pakistan. irfum3@gmail.com; mkhanbaloch@yahoo.com
[2]Department of Meteorology, COMSATS University Islamabad Tarlai Kalan, Park Road 45550, Islamabad Pakistan. jabir.syed@comsats.edu.pk
[3]Space and Upper Atmosphere Research Commission, Islamabad, Pakistan. m.shafiq.meteo@gmail.com
[4]Institute of Environmental Science and Engineering, School of Civil and Environmental Engineering, National University of Sciences and Technology, Sector H-12, Islamabad 44000, Pakistan. hamid_nust@yahoo.com
[5]Rawalpindi Waste Management Company, A-81, Iran Road, Satellite Town, Rawalpindi 46000, Pakistan
[6]Bio-Energy Testing and Analysis Laboratory (BETA Lab), Biological and Agricultural Engineering Department, Texas A&M University, College Station, TX 77843, USA. usman_hanif90@live.com
[7]Earth and Environmental Department. Bahria University Karachi Campus. nergisyasmin.bukc@bahria.edu.pk

Abstract

Glaciers in northern Pakistan are a prime source of freshwater, providing headwater in the Indus river system and serving as a lifeline to millions of people in the region. These glaciers undergo continuous changes by melting due to global warming or accumulation due to snowfall/precipitation at higher altitudes. In this study, we used remote sensing data to quantify glacier changes in spatiotemporal variability in the past three decades. Five glaciers in the Gilgit region (near the junction of the Hindukush and Karakoram Mountains) with an extent of less than 5 square kilometers were selected, namely Phakor glacier, Karamber glacier, East Gammu glacier, Bhort glacier, and Bad-e-Swat glacier. The fluctuations in these glaciers were monitored using a digital elevation model (DEM) and a cloud-free continuous series of Landsat satellite pictures from the minimal snow cover season. The annual climatic trends were studied through spatially interpolated gridded climate data WorldClim version-1 climate database for 1970 – 2000. We used it to study the variations of minimum and maximum temperature, solar radiation, and precipitation through the preparation of sub-sets from the original global grids. Because of its exact delineation in the Gilgit sub-basin, the characterized watersheds were visually compared to optical Landsat 8 OLI data for mountainous ridge matching, revealing that SRTM 30m (radar-based) demonstrated greater accuracy than other DEMs. The temporal assessment of Bhort, Bad-e-Sawat, East Gammu, Karamber, and other rivers was also carried out. It is observed that the glaciers in the Gilgit watershed are rather stable. The little variability of

glaciers is due to their geographic condition, altitude, topography, and orientation. Validation of the mapped glacier classes has been performed to check the accuracy assessment through an error matrix method. The kappa coefficient from the error matrix has been calculated to be 84 %. The study makes a critical input to a greater understanding of watershed controlling and hydrological processes in the upper Indus catchment's Gilgit watershed.

Keywords: Indus; Gilgit Watershed; Hydrological characteristics; glacier changes; Landsat

1. Introduction

The water cycle of Pakistan greatly depends on the freshwater supply from the Hindukush-Karakoram-Himalayas (HKH) through the Indus river system running from north to south across the country. Thus, the northern glaciers are an important part of the water cycle. Climate change affects the general accumulation and melting of the glaciers, which in turn impact human life and economy. Glaciers, at large, exist in remote mountainous rugged terrains and hence are difficult to monitor using field observations, these changes might be proficiently analyzed by remote sensing temporal or spatial analysis. The literature revealed that several pixels-based supervised and unsupervised classification methods are available to delineate the glacier ice.

Gilgit-Baltistan is located in the north of Pakistan, and geographically it is located in the north of Khyber Pakhtunkhwa province, south of Wakhan Corridor, south-west to China, and comprises an area of 72,971 km^2. With significant global climatic variations in last half-century (Vuille, et al. 2008), the temperature has increased from 0.32°C to 0.34°C per 10 years as associated with 0.10 °C per 10 years after 1939 (Vuille and Bradley, 2000).

Fresh water stored in the glaciers of the Gilgit basin in the Karakoram and Hindukush mountain ranges is an important source for water supply and irrigation in Pakistan, providing headwaters to the Indus River and other major rivers. Accelerating shrinkage of glaciers due to global warming adversely affect freshwater availability. region's climatologyDue to the difficulty in access and the

 doi:10.20944/preprints202211.0373.v1

large extent of glacier regions, field-based observations of climate parameters are difficult worldwide. Therefore, satellite-based Earth observation, providing repeat coverage at regular time intervals, is the main information source for studies and monitoring.

In the assessment of hydro-climatological fluctuations, flood risk management, watershed management, and water resource potential, morphometric studies of drainage networks are particularly valuable and possible (Ahmad et al., 2018). However, due to their widespread distribution across uneven terrain in the huge region, particularly in rocky places, it is difficult to examine all drainage networks through ground observations or surveys (Huggel et al., 2002). Highly developed methods such as (a) Digital Elevation Models (DEMs), (b) Shuttle Radar Topography Mission (SRTM), (c) Advanced Space-based Thermal Topography Mission, and (d) Global Elevation Model can be used to recognize drainage systems within basins and sub-basins (ASTER-GDEM). These DEMs were used to examine the drainage system, the Gilgit basin region, and the identification of micro-watershed boundaries. (Ali et al., 2017; Pareta and Pareta, 2014).

In Gilgit, the hydro-climatological discrepancies of the watershed of the Upper Indus sink are not as much of technically tacit due to various inaccessibility of the area, geography, and greater dissimilarities in climatic circumstances. Withdrawal of catchments at numerous gauges is a significant job in undertaking the watershed administration training. Geographical information technology (GIT) and satellite remote sensing (SRS) deliver an identical valuable technique to study watersheds.

There are many factors contributing to glacier mass loss besides climate warming; these are atmospheric circulation, cloud cover, rainfall, atmospheric particulate quantities, geo-morphology, and debris layer cover hence there are differences in the rate of ablation at different places (Yao et al., 2012; Racoviteanu et al., 2013). These factors, thus, pose a great deal of motivation to study the water shortages in South Asia (Klare, 2020).

This study aimed to review evaluate the climatetological factors in the Gilgit river basin in Pakistan and the seasonal variations of meteorological parameters. Temporal analysis of Bhort, Bad-e-Swat, East Gammu, Karamber, and Phakor Glaciers for a duration of 30 years last three decades ,is reported via multispectral TM, ETM+ and OLI satellite images.

Preprints (www.preprints.org) | NOT PEER-REVIEWED | Posted: 21 November 2022 doi:10.20944/preprints202211.0373.v1

2. Methodology

2.1. Study Area

Gilgit's watershed is a significant source in Pakistan's northern area (Figure1). The HKH region spans approximately 2,000 erkilometers throughout Southeast Asia and borders with Afghanistan, Bangladesh, Bhutan, China, India, and Nepal (Zhen and Li, 1998). The watershed is located between 72°25'02" E and 74°19'25" E, and 35°46'05" N and 36°51'16" N. The geographical watershed region is 13,552 square kilometres, with elevations ranging from 1,388 to 6,722 meters (Ali et al., 2017; 2019), and is redrawn in Figure 2 using elevation data from the Shuttle Radar Topography Mission (SRTM) at one arc-second resolution. Flash floods, supraglacial lakes, glacier lake outburst floods, and landslides are common in Pakistan's northern highlands (Kanwal et al., 2017; Qaisar et al., 2019; Rahim et al., 2018).

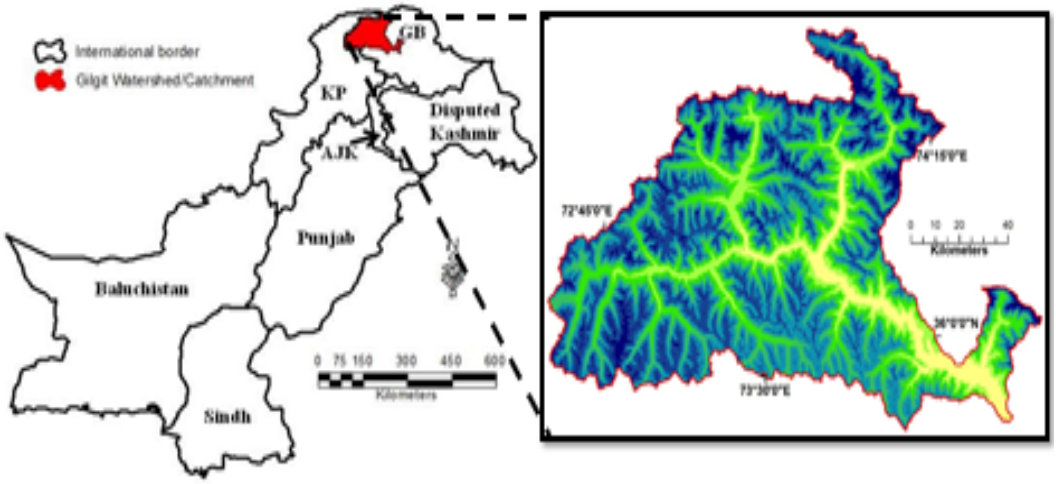

Figure 1: The study area elevation distribution

2.2. Climatological Data Analysis

Temperature and precipitation are the prime indicators of climate change, which are effectively contributing to the global climate system and energy cycle (Guan et al., 2022). The Gilgit basin, one of the UIB's sub-basins in the HKH region, is the focus of this study. The basin lies between the longitudes of 35°46′05″ to 36°1′16″ N and the latitudes of

Preprints (www.preprints.org) | NOT PEER-REVIEWED | Posted: 21 November 2022 doi:10.20944/preprints202211.0373.v1

72°25′02″ to 74°19′25″ E, spanning an approximate area of 12,726 km² with a mean elevation of 4,054 masl, according to the SRTM 30m digital elevation model (DEM) (Nazeer et al., 2022).

2.3. Glacier Change Analysis

There are three types of segmentation procedures: threshing/clustering, region-based, and edge-based. For object segmentation, two classifications were used: form and spectral pattern. The spectral pattern was given a higher weighting (70%) than the related form (30%) since it improves segmentation accuracy. The DEM images used for the study are shown in Table 1.

Table 1: Datasets used in this study

Satellite / Sensor	Year	Scene ID	Path	Row	Cloud Cover	Acquisition Date
Landsat 5 TM	1988	LT05_L1TP_150035_19881027_20170205_01	150	35	3%	1988-Oct-27
Landsat 5 TM	1994	LT05_L1TP_150035_19940708_20170113_01	150	35	4%	1994-Jul-08
Landsat 7 ETM+	1999	LE07_L1TP_150035_19990916_20170217_01	150	35	1%	1999-Sep-16
Landsat 8 OLI	2014	LC08_L1TP_150035_20140917_20170419_01	150	35	1.25%	2014-Sep-17
Landsat 8 OLI	2018	LC08_L1TP_150035_20180912_20180927_01	150	35	1.41%	2018-Sep-12

Overall Accuracy

By dividing the diagonal sum with the entire number of data points, the overall accuracy was computed.

$$Overall\ Accuracy\ = \frac{Diagonal\ Sum}{Total\ number\ of\ Sample\ Points}$$

Kappa Coefficient

The Kappa coefficient is a measurement of how well the categorization results compare to random values. It can have a range of values from 0 to 1. There is no agreement between the categorised image and the reference image if the kappa

 doi:10.20944/preprints202211.0373.v1

coefficient is 0. The categorised picture and the ground truth image are identical if the kappa coefficient is one. As a result, the larger the kappa coefficient, the better the categorization accuracy.

The accuracy of class identification has been tested in addition to overall accuracy. Classification mistakes are found in the non-diagonal cells of the matrix, which are instances where the reference picture and the categorized image do not match. Uncertainty (omission errors, omission) and overestimation are the two forms of errors (commission errors, commission).

Overestimation errors can occur for any class when a classification algorithm assigns pixels to a class that do not belong to it. The number of pixels incorrectly assigned to a class can be detected in column cells near the outer main diagonal of the class. The sum of these cell pixels is the absolute value of the class over-estimation, which is equal to 12 pixels in the first column on glacier class. Moreover, if we do division this sum by the total number of class pixels, we will get the relative over-estimation error (OvEr). For class 'glacier' denoted by 'G'.

$$OvEr = (bG + cG + dG) / \sum G$$

The Producer's accuracy (PrAc) indicator also describes the quantity of mistakes of over-estimation. It is the digit of properly recognized pixels divided by the total number of pixels in the reference image. For class 'glacier' denoted by 'G':

$$PrAc = aG / \sum G$$

OvEr and PrAc values are linked:

$$PrAc = 1 - OvEr$$

 doi:10.20944/preprints202211.0373.v1

Pixels that belong in one class are included in other classes, resulting in under-estimation mistakes for any class. The number of missed pixels is located in the row cells to the left and right of the main diagonal in the error matrix. Omission errors are highlighted in class G. The absolute (total) value of the class omission is the sum of these cells. In addition, we can calculate the relative (comparative) omission error by dividing this sum by the total number of class pixels in the classified image (OmEr):

$$OmEr = (aD + aW + aO) / \sum a$$

Another index that measures the quantity of omission mistakes is the user's accuracy (UsAc) (under-estimation). It's the number of successfully identified pixels in a class divided by the total number of pixels in the categorised image that belong to that class.

$$UsAc = aG / \sum G$$

OmEr and UsAc values are connected:

$$UsAc = 1 – Om$$

The overall accuracy of classification is represented by the kappa coefficient by including the values of OvEr and OmEr. It is vital to note that the accuracy numbers of the producer and user can't be utilised separately as a measure of categorization accuracy because they don't reveal the complete picture. Therefore, the user accuracy and producer accuracy are combined together into a random accuracy value (also termed as chance agreement value by some researchers). The random accuracy value is calculated to be 0.395.

Finally, the kappa coefficient is calculated from the following relationship.

 doi:10.20944/preprints202211.0373.v1

$$Kappa\ Coefficient = \frac{Overall\ Accuracy - Random\ Accuracy}{1 - Random\ Accuracy}$$

To summarise the technique, accuracy was assessed using an error matrix approach and a stratified random sampling method to provide 250 ground truth reference data points. For matching of the corresponding category, these ground truth locations were overlain on the land use land cover map. The generated error matrix and associated category membership resolute by ground truth, placed in the rows and classified cover type determined by this study methodology is placed in columns according to the methodology of Maitima et al., (2009). Correct values lie along the primary diagonal of the matrix when it is arranged this manner (Morgado et al., 2012). Classified values are incorrectly placed in the off diagonal sections of the matrix, making it obvious which class they belong to (Mukhopadhyay and Khan 2015).

3. Results and Discussions

3.1. Temperature profile of Gilgit Watershed

The global grids of monthly averaged 30-year data were obtained, and the study subset was extracted to obtain the regional temperature values. The interpolated minimum surface temperature processed from the point data from local stations portrays a high value of –0.2°C and a low value of –35.1°C for January. The low temperature values are mainly observed at higher altitudes on the Northern side and high values of temperature on the lower altitudes on the southeast of Gilgit watershed, respectively. The scale range is 60 km shown in Figure 2. Moreover, January, the severe winter month, has a more projecting T_{min} (low) compared to T_{max} (high). January is the frosty winter coldest month in Gilgit. February being the winter month has a more projecting T_{min} (low) as compare to T_{max} (high). The average high temperature in Gilgit rises slightly from a chilly January to a cool February, the last month of the winter. March is a pleasant month in Gilgit, with temperatures ranging from -13.3°C to 6.8°C on a mean. The mean high temperature in Gilgit climbs in March.

Preprints (www.preprints.org) | NOT PEER-REVIEWED | Posted: 21 November 2022 doi:10.20944/preprints202211.0373.v1

In Gilgit, April is a warm spring month, with average valley temperatures ranging from -7°C to -10°C. The average high temperature climbs in April. May, the penultimate month of spring, is another hot month in Gilgit, with an average valley temperature of 8°C. The average high temperature rises slightly from a moderately hot April to a warm May. June, the first month of summer, is a hot month in Gilgit. In Gilgit, July is the hottest month of the year. September is the first month of autumn and is still a hot month in Gilgit. October, like September, in Gilgit, is one warmer fall month. November is the last month of the fall, in Gilgit and is another weatherly relaxed month. December is a winter month in Gilgit with average min temperature fluctuating at -16°C.

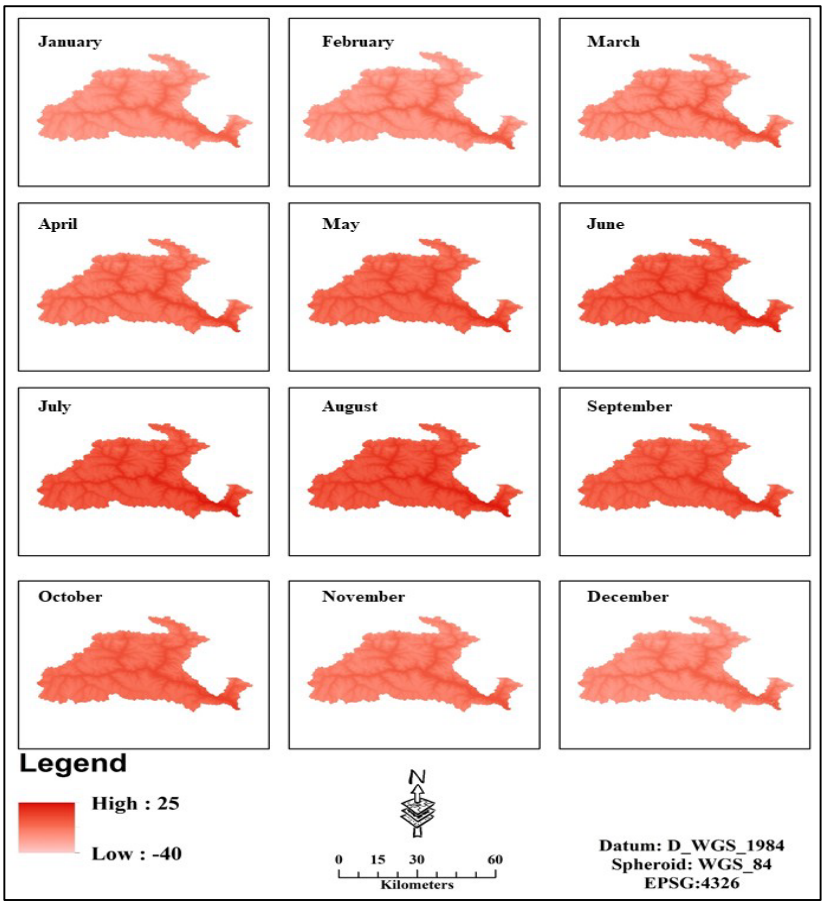

Figure 2: Spatial distribution of monthly averaged minimum temperature (in degrees Celsius) – Normalized matrix of yearly profile

3.2. Solar Radiation Intensity in the Gilgit Watershed

Radiation from the sun is the principle well spring of energy for the Earth's temperature framework. Changes in the Earth's circle around the sun cause contrasts in the cyclical circulation and measure of sunlight based radiation arriving at the earth. Chronicles of past environment show that there is a connection between these varieties and long haul environment changes. Interglacial

 doi:10.20944/preprints202211.0373.v1

conditions start with expanding mid-scope summer insolation and end as mid-scope summer insolation diminishes. Normal sunlight in March in Gilgit is 12 hours. June is the month with the most days (Average sunlight: 14.6h). December is the month with the shortest days (Average light: 9.8h). The longest day is 6 hours in March, while the shortest day is 6 hours in June (Average daylight: 10h). As shown in Figure 3, months with the least daylight are January, February and December when the typical daylight is 5 hours. The introduced sun powered radiation information handled from the point information from neighborhood stations, month to month arrived at the midpoint of 30 years, depicts a high worth of 7545kJ m-multi day-1 and a low worth of 5641 kJ m-multi day-1 across watershed for the long stretch of January. The low upsides of sun powered radiation at the higher heights on Northern side might be related with the huge measure of overcast cover frequently present at high mountains. Ordinarily, under clear sky conditions the sun oriented radiation increments with height. This is known as the height impact. The angle values are ~8% per 1000m of height.

Preprints (www.preprints.org) | NOT PEER-REVIEWED | Posted: 21 November 2022 doi:10.20944/preprints202211.0373.v1

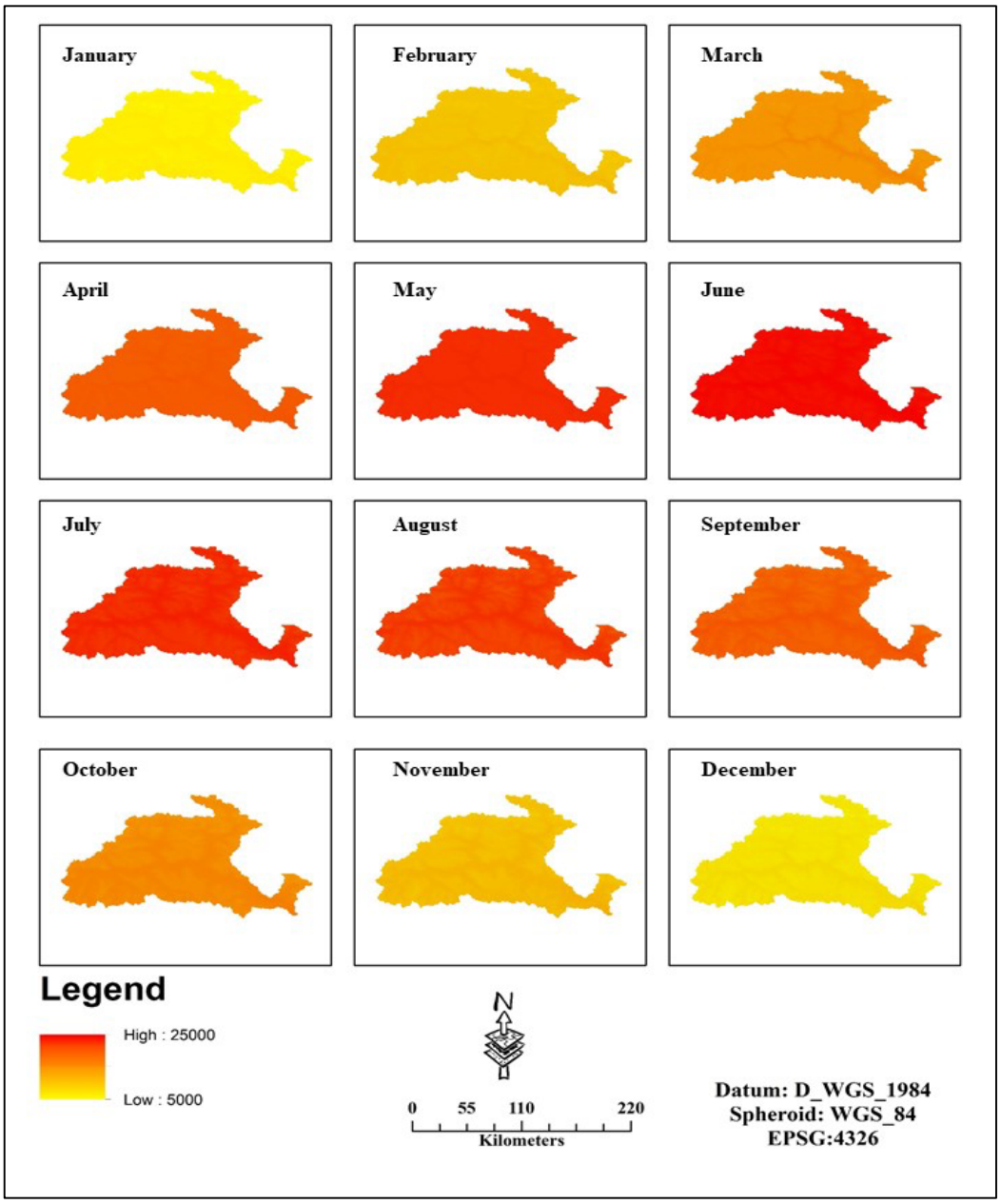

Figure 3: Spatial distribution of monthly averaged Solar radiation (in kJ m^{-2} day^{-1}) normalized matrix for yearly profile for Gilgit catchment

3.3. Precipitation in the Gilgit Watershed

There are four rainy seasons in the study area viz., wintertime, pre-monsoon, monsoon (rainy and cloud burst season) and post monsoon precipitation. The town of Gupis is known to have the lowest rainfall in the GB region (Javed et al., 2020). Javed et al., (2020) have analyzed the 90-years ground based point measurements from meteorological observatories operated by the Pak

Preprints (www.preprints.org) | NOT PEER-REVIEWED | Posted: 21 November 2022 doi:10.20944/preprints202211.0373.v1

Meteorological Department. However, the study lacks the interpolated analysis at the spatial extent. It is shown that Gupis station gets approx. 13 rainy days in the whole year excluding the solid precipitation in the form of snow at higher elevations.

The data of observation / measurement of precipitation are known to contain many inaccuracies owing to its spatial and temporal pattern in quantity and intensity. The interpolated precipitation data processed from the point data from local stations, monthly averaged of 30 years, shows values indicated in mapped in Figure 4.

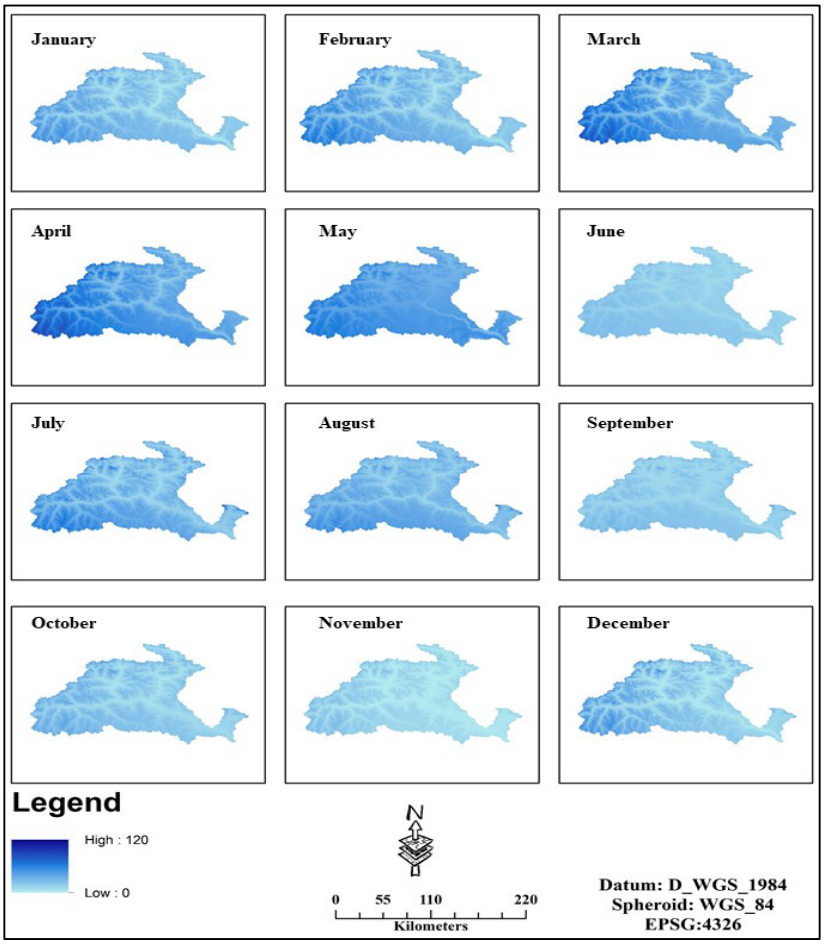

Figure 4: Spatial distribution of monthly precipitation (in mm) normalized matrix of yearly profile for Gilgit catchment

 doi:10.20944/preprints202211.0373.v1

3.4. Glacier Change Analysis

The glacier mapping using the object based classification techniques, thus, has been used to delineate the glacier area. The summary of the change detection for the five glaciers of the Gilgit watershed is explained in coming papragraphs. It was observed from the overall results that, mostly glaciers are rather stable specifically in the Gilgit watershed. The little variability of glaciers is due to their geographic condition, altitude, topography, orientation and climate conditions. In direction to evaluate the correctness of the glacier mapping the accuracy assessment was carried out using the error matrix approach with a calculated kappa coefficient value to be 84.14%.

3.4.1 Bhort Glacier Change Analysis

The extent coordinates of the Bhort glacier are from 74° 04′ 40′′ E to 74° 11′ 10′′ Eand from 36° 31′ 12′′ N to 36° 34′ 04′′ N. Elevation of the glacier goes upto 5,784 m and has a max slope of 57. It was observed that the ice-covered areas are 14.02, 10.87, 10.20, 9.65 and 9.91 km^2 for the years 1988, 1994, 1999, 2014 and 2018 respectively. However, the debris-covered area was 0.98, 2.23, 2.79, 2.86 and 2.45 km^2 for the years 1988, 1994, 1999, 2014 and 2018 respectively. Furthermore, the overall glacier changes are 15.00, 13.11, 13.00, 12.52, and 11.65 km^2 for the years 1988, 1994, 1999, 2014, and 2018, respectively. The results revealed that, the overall ice-covered area from 1988 to 2018 has reduced to 4.11 km^2. However, overall debris-covered area from 1988 to 2018 has increased to 1.47 sq km.

Preprints (www.preprints.org) | NOT PEER-REVIEWED | Posted: 21 November 2022 doi:10.20944/preprints202211.0373.v1

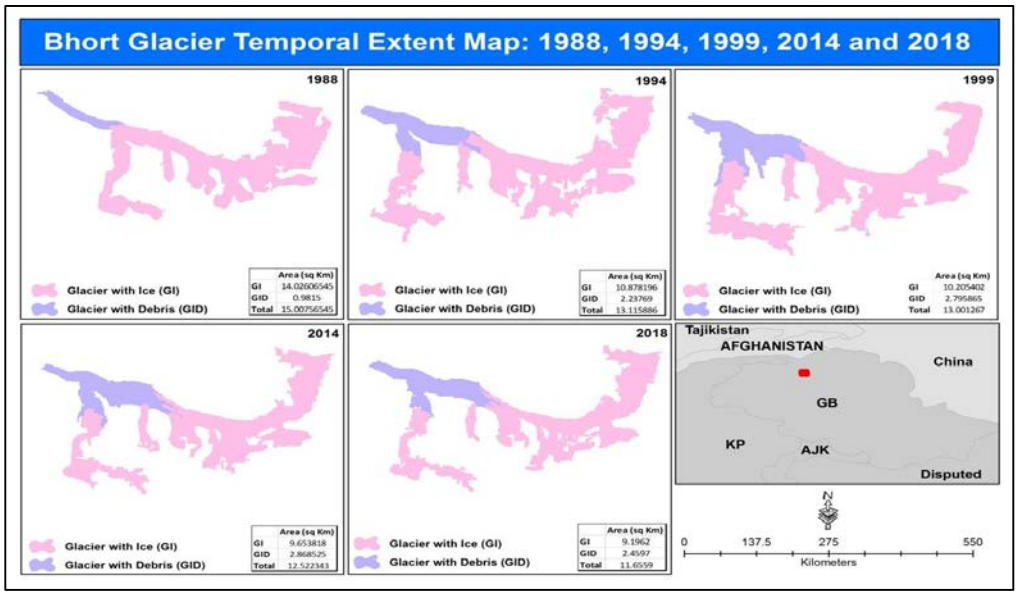

Figure 5: Bhort glacier temporal change extent for the years 1998, 1994, 1999, 2014 and 2018

3.4.2 Bad-e-Swat Glacier Change Analysis

The extent coordinates of the Bad-e-Swat glacier are from 74° 02′ 15′′ E to 74°06′ 35′′ E and from 36°28′ 15′′ N to 36° 32′ 20′′ N. Elevation of the glacier goes upto 5835 m and has a max slope of 51. It was observed that the ice-covered areas are 11.76, 14.13, 11.52, 12.72 and 11.67 sq km for the years 1988, 1994, 1999, 2014 and 2018 respectively. However, the debris-covered area was 0.48, 0.57, 1.007, 1.06 and 1.001 sq km for the years 1988, 1994, 1999, 2014 and 2018 respectively. Furthermore, the overall glacier changes are 12.24, 14.70, 12.52, 13.78 and 12.67 sq km for the years 1988, 1994, 1999, 2014 and 2018 respectively. The results revealed that, the overall ice-covered area for 30 years has been reduced in all years except 1988 that may be due to the climatic changes. However, the debris covered area from 1988 to 2018 has increased to 0.52 sq km.

Preprints (www.preprints.org) | NOT PEER-REVIEWED | Posted: 21 November 2022 doi:10.20944/preprints202211.0373.v1

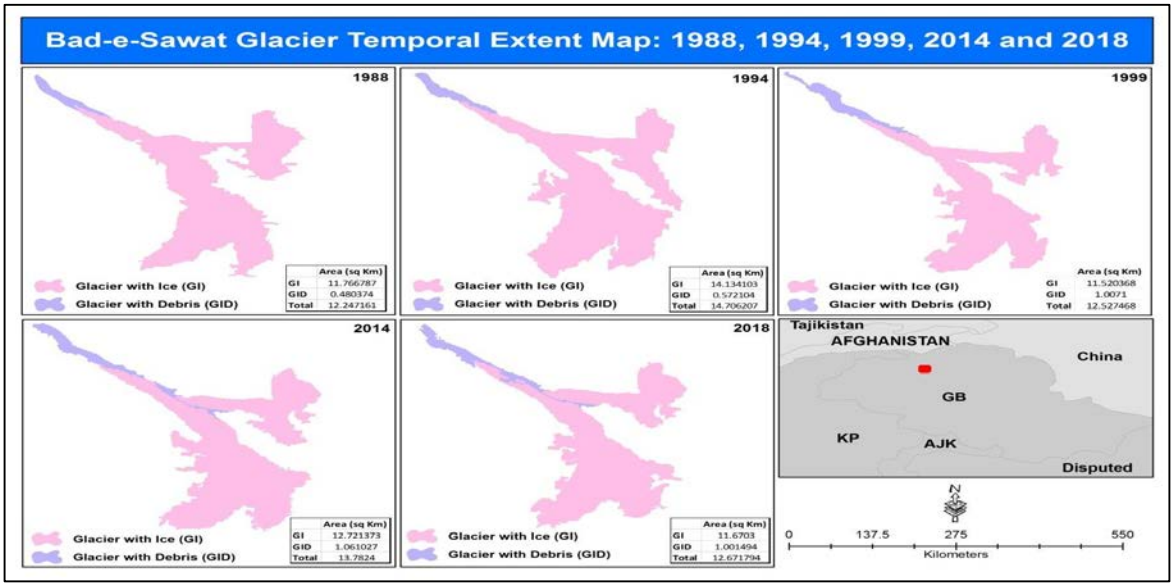

Figure 6: Bad-e-Swat glacier temporal glacier change extent for the years 1998, 1994, 1999, 2014 and 2018

3.4.3 East Gammu Glacier

The extent coordinates of the East Gammu glacier are from 73° 19′ 30′′ E to 73° 24′ 10′′ E and from 36° 35′ 10′′ N to 36° 38′ 30′′ N. Elevation of glacier goes upto 6379 m and has a max slope of 68. It was observed that the ice-covered areas are 9.02, 12.38, 11.47, 9.97 and 9.77 sq km for the years 1988, 1994, 1999, 2014 and 2018 respectively. However, the debris-covered area was 0.68, 0.63, 0.37, 0.47 and 0.32 sq km for the years 1988, 1994, 1999, 2014 and 2018 respectively. Furthermore, the overall glacier changes are 9.71, 13.02, 11.84, 10.44 and 10.09 sq km for the years 1988, 1994, 1999, 2014 and 2018 respectively. The results revealed that, the overall ice-covered area for 30 years has been reduced in all years except 1988 that may be due to the climatic changes. Moreover, the debris-covered area from 1988 to 2018 has decreased to 0.37 sq km.

Preprints (www.preprints.org) | NOT PEER-REVIEWED | Posted: 21 November 2022 doi:10.20944/preprints202211.0373.v1

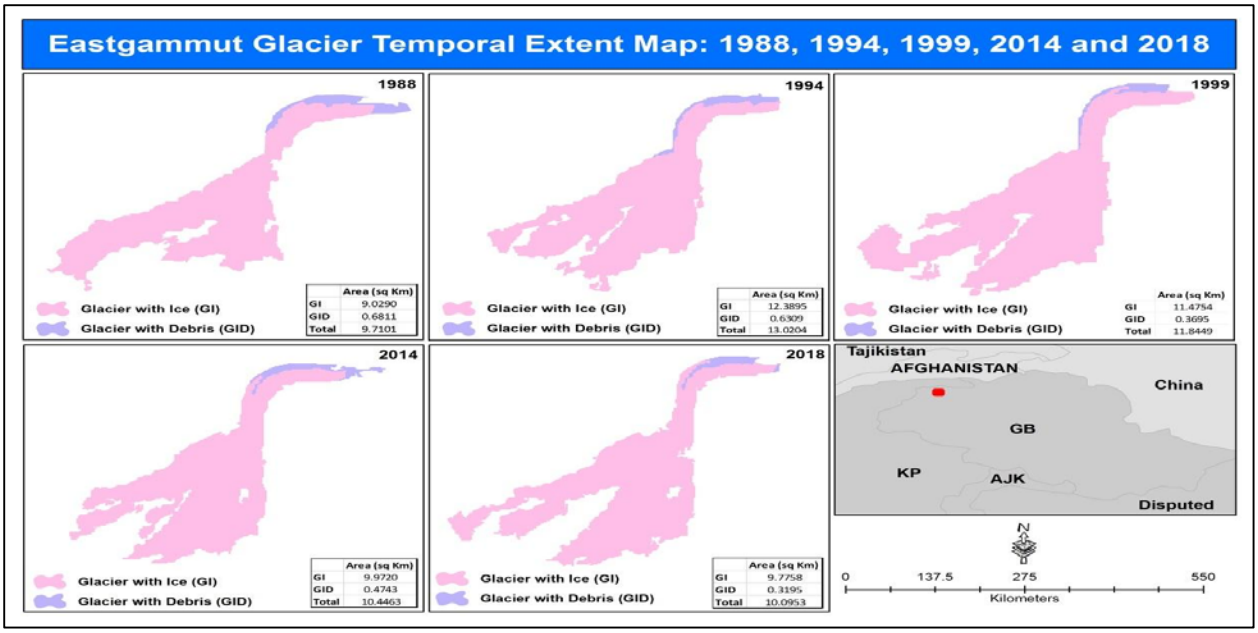

Figure 7: East Gammu glacier temporal change for the years 1998, 1994, 1999, 2014 and 2018

3.4.4 Karamber Glacier

The extent coordinates of the Karamber glacier are from 74°04′ 10′′ E to 74°17′ 50′′ E and from 36°33′ 45′′ N to 36°40′ 22′′ N. Elevation of glacier goes upto 6177 m and has a max slope of 74.1. It was observed that the ice-covered areas are 57.92, 58.03, 51.36, 51.26 and 52.18 sq km for the years 1988, 1994, 1999, 2014 and 2018 respectively. However, the debris-covered area was 5.33, 5.00, 8.00, 7.38 and 8.03 sq km for the years 1988, 1994, 1999, 2014 and 2018 respectively. Furthermore, the overall glacier changes are 63.26, 63.04, 59.36, 58.60 and 61.21 sq km for the years 1988, 1994, 1999, 2014 and 2018 respectively. The results revealed that, the overall ice-covered area from 1988 to 2018 has reduced to 4.74 sq km. However, overall debris-covered area from 1988 to 2018 has increased to 2.7 sq km.

Preprints (www.preprints.org) | NOT PEER-REVIEWED | Posted: 21 November 2022 doi:10.20944/preprints202211.0373.v1

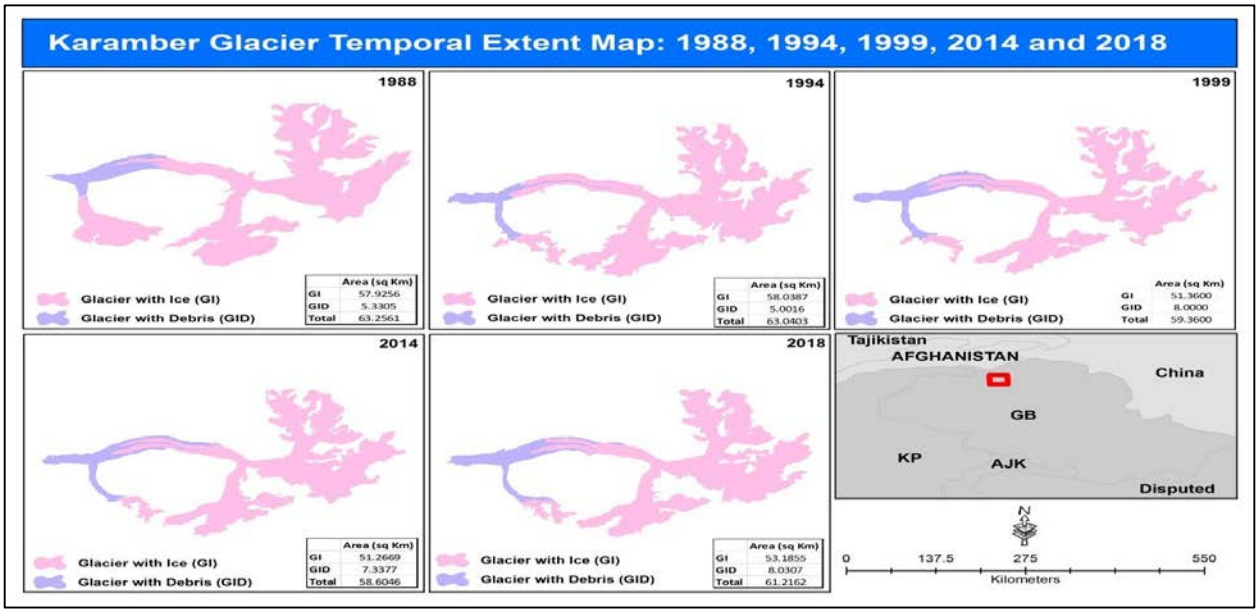

Figure 8: Karamber glacier temporal glacier change extent for the years 1998, 1994, 1999, 2014 and 2018

3.4.5 Phakor Glacier

The extent coordinates of the Bad-e-Swat glacier are from 73°59′ 26′′ E to 74°02′ 03′′ E and from 36°18′ 02′′ N to 36°20′ 55′′ N. Elevation of goes upto 5531 m and has a max slope of 74. It was observed that the ice-covered areas are 7.27, 7.02, 6.89, 6.32 and 6.14 sq km for the years 1988, 1994, 1999, 2014 and 2018 respectively. Moreover, no debris is found in the year of 1988.

However, the debris-covered area was 0.48, 0.16, 0.37 and 0.33 sq km for the years 1994, 1999, 2014 and 2018 respectively. Furthermore, the overall glacier changes are 7.27, 7.50, 7.06, 6.70 and 6.47 sq km for the years 1988, 1994, 1999, 2014 and 2018 respectively. The results revealed that, the overall ice-covered area from 1988 to 2018 has reduced to 1.17 sq km.

Preprints (www.preprints.org) | NOT PEER-REVIEWED | Posted: 21 November 2022 doi:10.20944/preprints202211.0373.v1

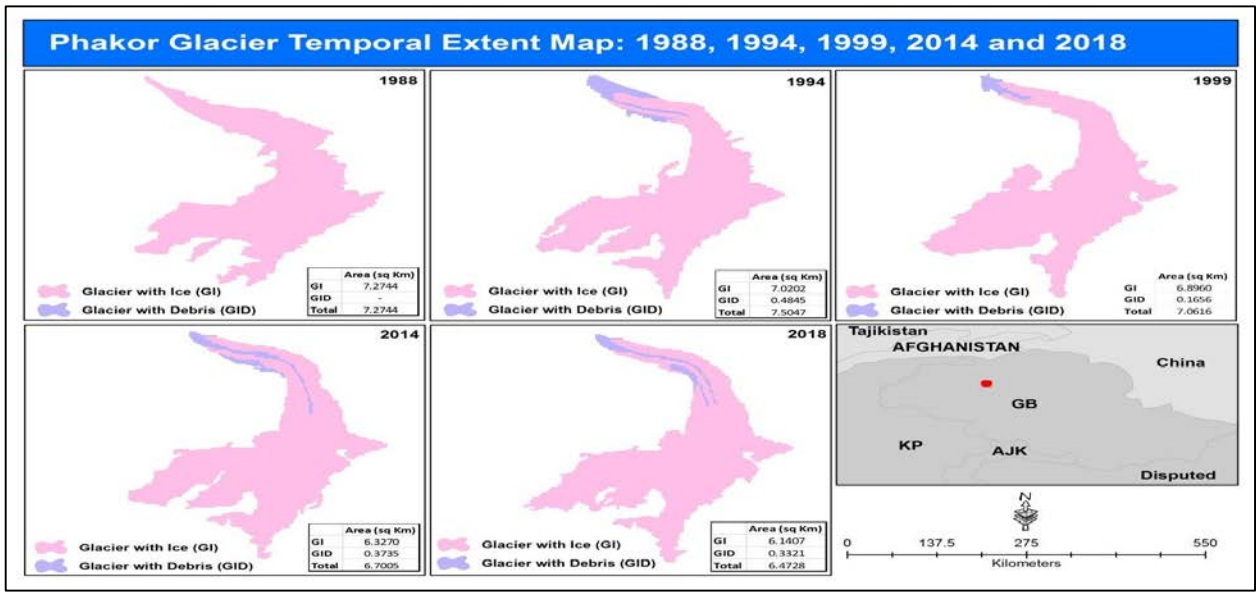

Figure 9: Phakor glacier temporal glacier change extent for the years 1998, 1994, 1999, 2014 and 2018

Figures 12, 13, and 14 shows the overall summary of the computed glacier areas. Figure 12 shows the aireal extend of the glacier area without debris cover glacier i.e., only clear ice glacier has been mapped. The debris cover part of the 5x glaciers have also been mapped and the covered area is shown in Figure 13. Figure 14 shows the sum of clean ice glacier and debris covered glacier to assess the complete extent of the glacier.

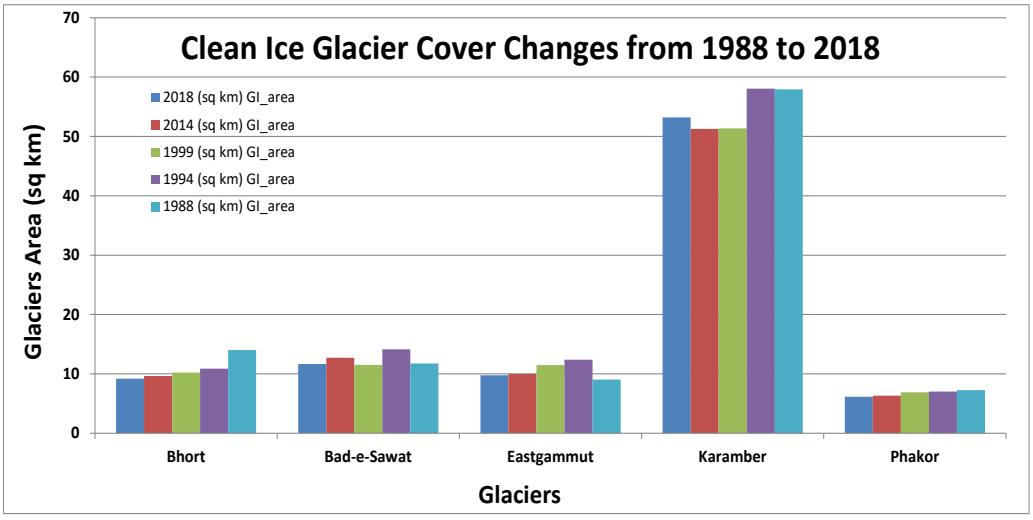

Figure 10: Glacier-wise change trends for clean ice

Preprints (www.preprints.org) | NOT PEER-REVIEWED | Posted: 21 November 2022 doi:10.20944/preprints202211.0373.v1

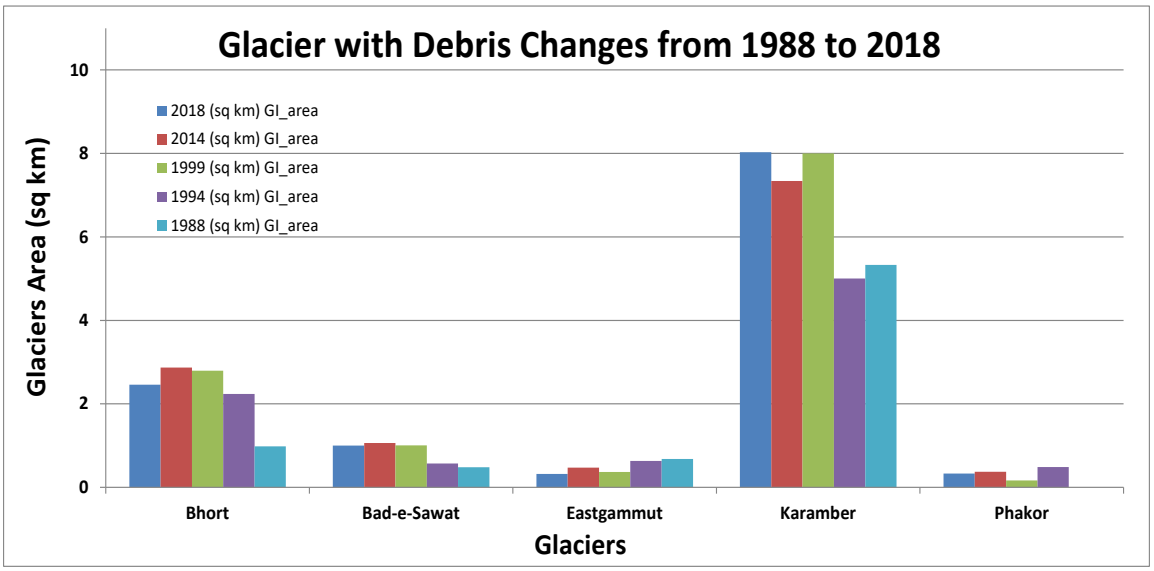

Figure 11: Glacier-wise change trends for debris covered ice Tabular Presentation of Glacier Cover Area (GCA)

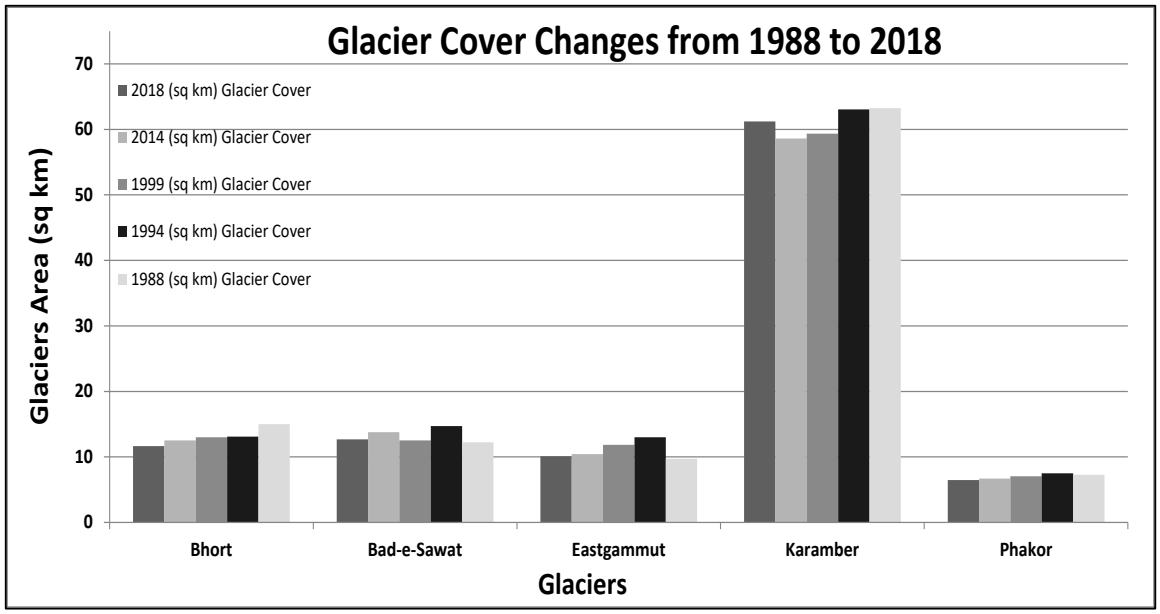

Figure 12: Glacier-wise change trends

Preprints (www.preprints.org) | NOT PEER-REVIEWED | Posted: 21 November 2022 doi:10.20944/preprints202211.0373.v1

3.5 Accuracy Assessment on Mapping of Glaciers

3.5.1 Error Matrix

Any classification system used to comprehend a remotely sensed image will always produce some level of inaccuracy. In order to assess the inaccuracies, the simplest way is the pictorial inspection. We can see mistakes and estimate their size by equating the image with the results of its interpretation. However, in order to have a reliable accuracy assessment, it is imperative to utilize numerical methods of valuation.

A confusion matrix (or error matrix) is a common quantitative tool for determining picture categorization accuracy. A table shows how the categorization result and a reference image correspond. The ground veracity data gathered during the field survey was used to build the error matrix. These data include, (a). Cartographic information and (b). The results of the ground survey were recorded using a GPS receiver. Table 7 shows the error matrix that was computed. The ground truth classes are in the table's columns, and the classes of the categorised image to be assessed are in the table's rows. The number of pixels for all conceivable correlations between the ground truth and the categorised image are shown in the table's cells.

Table 8: Error matrix

Class	Glc	Debris	Water bodies	Other (rocks etc)	Row Total	User Accuracy (UsAc) [on a scale of 0 – 1]
Glacier Cover	133	6	0	3	142	0.937
Debris Cover	8	35	0	0	43	0.814
Water Bodies	0	0	20	1	21	0.952
Other (rocks etc.)	4	0	2	38	44	0.864

 doi:10.20944/preprints202211.0373.v1

Col Total	145	41	22	42	250	
Producer Accuracy (PrAc) [on a scale of 0 – 1]	0.917	0.854	0.909	0.905		

Overall Accuracy: 87.50%

Kappa Coefficient= 79.99% ≈ 80%

The diagonal essentials of the matrix have been shaded and highlighted. The number of accurately detected pixels is contained in diagonal cells. The entire number of pixels has been divided by the sum of these pixels to give the overall classification accuracy 'p(a)', which is equal to 87.50 percent.

4. Conclusions

The study investigated glacier movements from 1988 to 2018 utilising remote sensing data for five glaciers (each having an area of less than 5 km^2) in the Karakoram region's Gilgit river basin. Glacier differences were calculated based on standard areal extent measured through object-oriented classification with the help of Landsat satellite imagery. Watershed extraction was carried out by using SRTM radar data with standard procedure on computation of flow directions and flow accumulation. The change detection of the glacier area in the last three decades has been carried out. In order to, accomplish the task the satellite imageries from year 1988, 1994, 1999, 2014 and 2018 have been used to map and monitor the 5 large glaciers in the Gilgit watershed, viz., Bhort, Bad-e-Swat, East Gammut, Karamber and Phakor Glaciers. At first, the un-supervised classification techniques were applied, the results obtained were not so much accurate with visible misclassification of several glacier cover areas. The overall accuracy was improved by the supervised classification. The glacier mapping using the supervised classification techniques, thus, have been used to delineate the glacier area. It was observed from the overall results that, mostly glaciers remained rather stable in the Gilgit watershed. The little variability of glaciers is due to their geographic condition, altitude, topography, and orientation.

5. Acknowledgements

The first author appreciates the help of the staff at Bahria University Karachi Campus, Pakistan's Department of Earth and Environmental Science. The authors are grateful to the USGS for making Landsat and elevation data available. The authors are grateful to the anonymous reviewers whose recommendations and comments helped to improve the manuscript greatly.

REFERENCES

Ahmad, S., Israr, M., Liu, S., Hayat, H., Gul, J., Wajid, S., et al. (2018). Spatio-temporal trends in snow extent and their linkage to hydro-climatological and topographical factors in the Chitral River Basin (Hindukush, Pakistan). *Geocarto International*, 1-24.

Ali, K., Bajracharya, R. M., Chapagain, N. R., Raut, N., Sitaula, B. K., Begum, F., et al. (2019). Analyzing Land Cover Change Using Remote Sensing and GIS: A Case Study of Gilgit River Basin, North Pakistan. *International Journal of Economic and Environmental Geology*, **10**(1), 100-105.

Ali, K., Bajracharya, R. M., Sitaula, B. K., Raut, N., and Koirala, H. L. (2017). Morphometric Analysis of Gilgit River Basin in Mountainous Region of Gilgit-Baltistan Province, Northern Pakistan. *Journal of Geoscience and Environment Protection*, **5**(07), 70.

Huggel, C., Kaab, A., Haeberli, W., Teysseire, P., and Paul, F. (2002). Remote sensing based assessment of hazards from glacier lake outbursts: a case study in the Swiss Alps. *Canadian Geotechnical Journal*, **39**(2), 316-330.

Javed, ZH., Khan, S., Wahid, A., Ranjha, A. N., Hasan, M., (2020). Climate of the Gilgit-Baltistan Province, Pakistan. International Journal of Economic and Environmental Geology,**11**(3), 16-21.

Kanwal, S., Atif, S., and Shafiq, M. (2017). GIS based landslide susceptibility mapping of northern areas of Pakistan, a case study of Shigar and Shyok Basins. *Geomatics, Natural Hazards and Risk*, **8**(2), 348-366.

Klare, M. T. (2020). Climate Change, Water Scarcity, and the Potential for Interstate Conflict in South Asia. *Journal of Strategic Security*, **13**(4), 109-122.

Maitima, J.M., Mugatha, S.M., Reid, R.S., Gachimbi, L.N., Majule, A., Lyaruu, H., Pomery, D., Mathai, S. and Mugisha, S., (2009). The linkages between land use change, land degradation and biodiversity across East Africa. African Journal of Environmental Science and Technology,**3**(10).

Morgado, P., Toger, M., Abrantes, P., & Fiegel, J. (2012). A bottom up approach to modeling habitat connectivity dynamics through networks analysis. *Sustainable Development–Authoritative and Leading Edge Content for Environmental Management*, 131-148.

Mukhopadhyay, B., and Khan, A. (2015). A reevaluation of the snowmelt and glacial melt in river flows within Upper Indus Basin and its significance in a changing climate. *Journal of Hydrology*, **527**, 119-132.

Nazeer, A., Maskey, S., Skaugen, T., & McClain, M. E. (2022). Simulating the hydrological regime of the snow fed and glaciarised Gilgit Basin in the Upper Indus using global precipitation products and a data parsimonious precipitation-runoff model. *Science of the Total Environment*, **802**, 149872.

 doi:10.20944/preprints202211.0373.v1

Pareta, K., and Pareta, U. (2014). New watershed codification system for Indian river basins. *Journal of hydrology and environment research*, **2**(1), 31-40.

Qaisar, M., Shafiq, M., Ghauri, B. M. K., Younes, I., and Abuzar, M. K. (2019). Comparative Analysis of Different Remote Sensing Techniques for Mapping of Supraglacial Lakes on Hispar Glacier. *International Journal of Economic and Environmental Geology*, **9**(2), 66-74.

Rahim, I., Ali, S. M., and Aslam, M. (2018). GIS Based landslide susceptibility mapping with application of analytical hierarchy process in District Ghizer, Gilgit Baltistan Pakistan. *Journal of Geoscience and Environment Protection*, **6**(2), 34-49.

Racoviteanu, A. E., Armstrong, R., & Williams, M. W. (2013). Evaluation of an ice ablation model to estimate the contribution of melting glacier ice to annual discharge in the Nepal Himalaya. *Water Resources Research*, **49**(9), 5117-5133.

Vuille, M., & Bradley, R. S. (2000). Mean annual temperature trends and their vertical structure in the tropical Andes. Geophysical Research Letters, **27**(23), 3885-3888.

Vuille, M., Francou, B., Wagnon, P., Juen, I., Kaser, G., Mark, B. G., & Bradley, R. S. (2008). Climate change and tropical Andean glaciers: Past, present and future. Earth-science reviews, **89**(3-4), 79-96.

Yao, T., Thompson, L., Yang, W., Yu, W., Gao, Y., Guo, X., ... & Joswiak, D. (2012). Different glacier status with atmospheric circulations in Tibetan Plateau and surroundings. *Nature climate change*, 2(9), 663-667.

Zhen, X., and Li, J., (1998). Remote Sensing monitoring of glaciers, snow and lake ice in *Qinghai-Xizang (Tibetan) Plateau and their Influence on Environments*, edited by M. Tang, G. Cheng and Z. Lin (Guangzhou, China: Guandong Sciences and Technology Press) pp.279-308.